The Study of Air Flows for an Electric Motor with a Nozzle for an Unmanned Flying Platform

Lucjan SETLAK, Rafał KOWALIK and Stanisław BODZON
Aviation Division, Department of Avionics and Control Systems
Polish Air Force University
Deblin 08-521, ul. Dywizjonu 303 No. 35
POLAND
l.setlak@law.mil.pl, r.kowalik@law.mil.pl, s.bodzon3603@wsosp.edu.pl

Abstract: - The subject of this article is the analysis of unit parameters of the electric motor placed on the rotorcraft carrying frame in the aspect of the process implemented in this type of drive unit. The main purpose of this work is to carry out tests of the air flow of the drive unit in the range of changes in the unit thrust depending on the operating conditions of electric motors, based on numerical analyses using the finite element methods, through which the analysis of the nozzle installed under the engine was performed. To this end, the course of changes in calculated parameters characterizing aerodynamics along flow channels of engines implemented in unmanned aircraft vehicles was analyzed. In addition, created mathematical models describing physical phenomena within the simulation domain (study area) were considered. In the final part of the article, on the basis of the above and the obtained results of simulation studies, practical conclusions were formulated.

Key-Words: - Study, airflows, electric motor nozzle, unmanned aerial vehicles, finite element methods (FEM)

1 Introduction

Currently, in unmanned flying platforms, depending on their type, size and purpose, various types of power units are implemented, including electric motors, combustion piston and turbine engines, as well as turbine jet engines. These teams play an important role in the field of modern means of transport and form the basis of their operation, based on the conversion of energy contained in the primary energy carrier into useful work [1], [2].

The key problems in the implementation of tasks at the design stage of unmanned aerial vehicle, which must be faced by the constructors of aviation power units, are first of all the correct selection of the drive unit, thanks to which it is possible to achieve high efficiency with the lowest unit weight.

Accepting purpose and the functionality and requirements of the UAV *(Unmanned Aerial Vehicle)* object, as the basic input data at the initial stage of testing electric engine of the propulsion unit, it can be noticed that the type of engine proposed depends on the adopted criteria for the tasks performed by the unmanned flying platform.

For example, a UAV object as a flying target (high speed requirement), for reconnaissance (long range and flight altitude requirement) or for military use, e.g. reconnaissance of the opponent's battlefield (requirement of unnoticeability and low speed and flight altitude) [3], [4].

Proper selection of the power unit consists in the selection of the most effective solution, among various possibilities, i.e. those that will allow the best use of the aerodynamic characteristics of the rotorcraft for the purpose of generating a proper thrust force for the power unit in terms of the requirements of the potential design.

In addition, the reliability that ensures the safety of aircraft operation also plays an important role. The process of both designing and constructing air internal combustion engines with the required high power in the context of the required engine thrust and possibly light construction determined the development and performance of flying objects.

Modern aviation engines as advanced propulsion units undergo various tests in order to obtain appropriate operational characteristics, obtained by using analytical and experimental methods. The forecasted and desirable directions for the development of drive units of UAV objects include the need to increase their efficiency and reliability, reduce weight, unit fuel consumption and the ability to receive more power for the needs of powering the on-board equipment [5], [6].

Therefore, for example, to reduce the detectability of an aircraft, both the propulsion unit and the rotorcraft should be more effectively integrated, as well as reduce the infrared radiation emitted by the engine. At the stage of designing the drive unit, the constructors are obliged to take into

account the specific operating conditions of unmanned aerial vehicles, in which long-term operations are performed with a relatively small number of engine start-up and shutdowns.

It is also planned to implement electric motors powered by fuel cells, which are more efficient energy sources compared to traditional battery packs. It is also important to reduce the noise generated by the power unit, and what is related to protect the environment.

One of the trends in the dynamic development of turbine jet engines is the reduction of their dimensions. The miniaturization process of this kind of propulsion units was commonly associated with the use of hobby or selected military targets, however, nowadays more and more interest in a wider range of applications can be observed, e.g. using unmanned flying platforms [7].

This is probably dictated by the use of this type of engines for the propulsion of unmanned aerial vehicles as well as small electric generators or hybrid drives. However, undoubtedly, the key issue in the jet engine category is their mass, the value of which is inversely proportional to their dimensions, i.e. the larger their external dimensions, the lower the mass, the engines of which are characterized by the same or greater thrust with less own weight.

This is mainly due to the relatively light alloys used in the construction process during the production of individual engine components, characterized by the ability to transfer mechanical stresses at high operating temperatures, as a result of which these types of alloys are free from creep phenomena, i.e. the tendency to change shape together with temperature changes.

In the case of the UAV object, electric drives are used by constructors in the multi-rotor construction. In this case, multistage structural solutions are ineffective due to the occurrence of the friction phenomenon in the boundary layer of the motor flow channels, causing pressure losses and in terms of control [8], [9].

In view of the above, the paper presents the results of simulation tests, determining the change of air flow for an electric drive unit with a nozzle.

2 Components of the Drive Unit of the UAV Object

The design of the proposed power unit of the UAV object is equipped into a brushless electric motor together with speed controller and control unit and nozzle. The model of engine operation is based on the dynamics of individual components included in its composition and physical phenomena in the scope of the ability to store and convert energy in its components.

In the case of the nozzle spraying the engine exhaust air, isentropic processes are taken, which significantly affect the aerodynamics of the flying platform.

Key components included in the considered configuration of the drive unit of the unmanned flying platform, analyzed in simulation tests are shown in the figure below (Fig. 1).

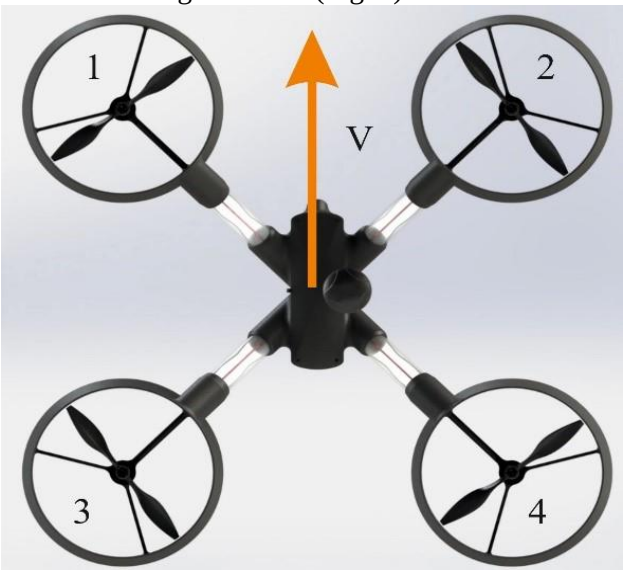

Fig. 1 Construction of the drive unit of the unmanned flying platform

Each component of the electric motor is described by a steady-state characteristic and then by a volume of the determined domain in which the air and energy resistances are stored.

A mathematical model defining the physical phenomena of aerodynamics of an electric motor with the nozzle is based on an approach based on the collective behavior of dynamic components that are part of the propulsion system of the unmanned flying platform based on non-stationary one-dimensional physical laws described by means of a set of first-order differential equations and basic algebraic relations [10], [11].

The nozzle is an important element of the electric engine of the power unit, in which there is a change of air resistance, which affects the dynamics of the flying platform. It should be noted that the construction parameters of the nozzle, with the adopted structure with a larger working surface, have a decisive influence on the performance characteristics of the engine, i.e. both on the working pressure and its thrust force.

Designing a nozzle unit is therefore one of the most responsible stages of developing a structural solution for the drive unit. Therefore, in the light of

the above, it seems advisable to indicate what kind of problems associated with the development of the nozzle unit can be encountered by the potential engineers of the electric motor at the design stage.

The next part of this paper presents the next stages of simulation tests of the drive unit with the nozzle [12], [13].

2.1 Nozzle

In the process of modelling of electric the motor of the power unit intended for the UAV object, a nozzle was adopted. Partially expanded air coming from the propeller at relatively high pressure is accelerated to a high velocity at the tip of the nozzle.

In the final stage, the gases expand to ambient pressure and provide thrust force to propel the flying platform. The gas flow in the nozzle is also considered a quasi-stable state, analogously to the inlet analysis considered, and therefore the dynamics in the nozzle was not taken into account.

Modelling converged nozzle for a tunnel motor is based on the following mathematical equations. The mass air flow rate through the nozzle depends on two factors: the back pressure in the nozzle and the critical outlet pressure of the nozzle.

For the purpose of creating mathematical models of the proposed solution, the concept of tunneling in the conducted simulation studies is understood in the context of the simulation domain in the area of research [14], [15], [16].

Considering the above, for a certain inlet pressure to the nozzle there is a critical back pressure determined by the following expression (1):

$$P_{nuzzle} = \left[\frac{2}{\gamma_b + 1}\right]^{\frac{\gamma_b}{\gamma_b - 1}} \cdot P_{inlet} \tag{1}$$

Depending on the value of the critical pressure occurring on the tunnel engine nozzle and its flow around the nozzle, the analysis considered for two cases can be made.

Case 1. If the back pressure appearing on the nozzle is greater than the critical pressure generated in the tunnel encapsulation, the air flow at the nozzle exit is considered uniform, this PCR output pressure is equal to the back pressure P_B ($P_B > P_{CR}$).

The basic values of the parameters in the form of flow rate, velocity at the output and produced thrust force in the tunnel casing are calculated using the following expressions [17], [18].

The pressure output from the nozzle with increased length in the tunnel motor was defined as (2):

$$P_{out} = P_B \tag{2}$$

In turn, the mass air flow around the nozzle is expressed as follows (3):

$$m = \frac{P_n}{\sqrt{RT}} A \left[\frac{P_{out}}{P_n}\right]^{\frac{1}{\gamma_b}} \cdot \sqrt{\frac{2}{\gamma_b + 1} \cdot \left[\frac{P_{out}}{P_n}\right]^{\frac{\gamma_{b-1}}{\gamma_b}}} \tag{3}$$

where:

- R- radius of the tunnelling housing;
- A- cross-sectional tunnelling view;
- T- temperature inside the tunnel;
- P_n- pressure around the nozzle.

However, the created thrust force on the nozzle can be described by the mathematical dependence (4):

$$m = C_v m \cdot \sqrt{2C_p T \cdot \left[1 - \left(\frac{P_{out}}{P_n}\right)^{\frac{\gamma_{b-1}}{\gamma_b}}\right]} \tag{4}$$

where: Cv and Cp- determine compressed air temperature values outside the tunnel and inside it, respectively.

The mathematical dependence on the velocity of the jet at the outlet of the nozzle in the driving unit of the unmanned flying platform was recorded as (5):

$$V_e = \sqrt{\frac{2}{\gamma_b + 1} RT \cdot \left[1 - \left(\frac{P_{out}}{P_n}\right)^{\frac{\gamma_{b-1}}{\gamma_b}}\right]} \tag{5}$$

Case 2. If the back pressure at the nozzle is less than the critical pressure, the flow is resonant or throttled at the outlet, and the outlet pressure is equal to the critical pressure. The flow rate, output speed and generated thrust force are calculated from the following mathematical expressions [19], [20].

Thus, if ($P_B < P_{CR}$).

The pressure output from the nozzle with increased length in the tunnel motor is defined by (6):

$$P_{out} = P_B \tag{6}$$

In turn, the mass air flow around the nozzle is expressed as follows (7):

$$m = \frac{P_n}{\sqrt{RT}} A \cdot \sqrt{\gamma_b \cdot \left[\frac{2}{\gamma_b + 1}\right]^{\frac{\gamma_{b-1}}{\gamma_{b-1}}}} \tag{7}$$

where:

- R- radius of the tunnelling housing;
- A- cross-sectional tunnelling view;
- T- temperature inside the tunnel;
- P_n- pressure around the nozzle.

However, the created thrust force on the nozzle can be described by the mathematical dependence (8):

$$m = C_v m \cdot \sqrt{2C_p T \cdot \left[1 - \left(\frac{P_{out}}{P_n}\right)^{\frac{\gamma_{b-1}}{\gamma_b}}\right] + A[P_B + P_{out}]} \quad (8)$$

where: Cv and Cp- determine compressed air temperature values outside the tunnel and inside it, respectively.

The mathematical dependence on the velocity of the jet at the outlet of the nozzle in the driving unit of the unmanned flying platform was recorded as (9):

$$V_e = \sqrt{\frac{2\gamma_b}{\gamma_b + 1} RT \cdot \left[1 - \left(\frac{P_{out}}{P_n}\right)^{\frac{\gamma_{b-1}}{\gamma_b}}\right]} \quad (9)$$

The basic components of an electric power unit include: a propeller and a motor, forming an integrated propeller-motor unit, a power source in the form of a battery and an engine speed controller.

2.2 The propeller-engine unit

The basic element of the unit is a propeller, which is individually adjusted, taking into account key criteria in the scope of basic technical parameters in the form of: max. engine power and speed, engine efficiency having an impact on lower energy consumption and a key parameter, which is the weight of the propeller-engine unit.

The cooperation between the propeller and the engine takes place in the context of adapting the power consumed to the generated thrust generated during operation of the electric propeller-motor unit.

The cooperation between the propeller and the engine takes place in the context of adapting the power consumed to the generated thrust force generated during operation of the electric propeller-motor unit.

For example, with the right selection of a propeller with the same diameter and larger stroke, more power can be obtained, necessary for the thrust force generated by the power unit with an electric motor.

In turn, in the case of engine adaptation, special attention should be paid to the change in the efficiency of the electric motor depending on the type of propeller used [21], [22].

Thus, the essence of cooperation of the integrated propeller-electric unit is that the change of the type of propeller leads to a change in the performance of the power unit, and the change of the electric motor, for example in the power range, changes the thrust force received on the propeller.

2.3 Power source in the form of a storage battery

Another component of the electric drive unit is the power source in the form of a battery. In current solutions of miniaturization on unmanned aircraft, a power module is used, based on three or four cells of galvanic lithium-polymer batteries (LiPo) with a nominal voltage of 11.1/14.8 V, able to provide the appropriate quality of electricity to receivers, such as a powerplant, flight controller and other additional equipment mounted on the unmanned aerial object [23], [24], [25].

In the selection of the power source, the key parameters of the batteries should be taken into account, among others: capacity, mass, max. allowable value of the discharging current, whose main purpose is to ensure the implementation of tasks during the flight.

The principle of battery operation is based on the generation of electricity due to chemical reactions occurring in the battery during the charging and discharging process.

It should be noted that the maximum flight time of an unmanned flying platform must be long enough to allow a full operation with the included reserve.

In view of the above, the proper selection of a battery is in the context of the proposed in this work, the structural solution of the electric drive unit of the unmanned flying platform will depend on the thrust-generating elements, such as the power unit and on-board aircraft equipment.

Another, also important parameter required in the selection of the appropriate battery pack is the current efficiency coefficient, which will allow the proper operation of the drive unit by appropriate selection of this parameter[26], [27].

At the same time it should be mentioned, which is obvious, that the largest current consumed will be at the start, because during this maneuver, the drive unit must generate the greatest thrust force.

2.4 Engine rotational speed controller

The next component of the electric drive unit of the UAV object is the ESC speed controller *(Electronic Speed Controller)*.

Electronic speed controller module is an electronic system used to control and regulate the rotational speed of an electric motor. It can also enable reverse rotation of the motor and its dynamic braking [28], [29], 30].

Its main purpose is to transform the control signal obtained from a measuring and control unit, e.g. in the form of an electronic module with a built-in microcontroller, to the appropriate value and frequency of the voltage allowing the proper functionality of the electric motor operation at the set preset speed.

When choosing a speed controller, the following parameters must be taken into account:

- type of UAV object;
- engine type;
- maximum and instantaneous value of electric current;
- cooperation with a flight controller;
- required motor current;
- voltage and battery type.

In a big simplification the speed control is adjusted to the frequency of the 3-phase inverter (in the case of a 3-phase motor), the higher the frequency, the faster the synchronous motor speed is.

The essence of the work of the regulator is that the controller being in the selected programming mode generates a series of sounds that are key parameters of the regulator, and the output from a specific mode after selecting a series of pulses means choosing the appropriate regulator option.

In view of the above, it should be noted that the ESC regulator is a universal device, i.e. that the microcontroller built in the ESC system has the ability to perform much more functions than just direct regulation of the rotational speed of the considered engine [31], [32].

In addition, it should be noted that the regulator is individually selected depending on the type of motor used, such as the brushless DC motor BLDC *(Brushless DC Motor)*, where the key parameters are the type of output current in the form of direct current or 3-phase alternating current, as well as depending on the max. value of the current drawn in the system and the type of voltage of the power module with which the engine speed controller can work.

3 Mathematical Model of Dynamics of a 4-rotor Unmanned Flying Platform

Making a mathematical modeling of a multi-rotor UAV object, based on a 4-rotor unmanned flying platform in the context of the control it should be noted that the creation of a dynamic model of unmanned aerial vehicle, with particular reference to selected simulation tests is required due to to carry out tests both in the field of navigation and control in a closed rotom [33], [34].

The proposed model of equations, illustrating the specific properties and location of a 4-rotor UAV object, represents a construction unchanging in the context of rotation, characterized by six degrees of freedom and four entrances.

The dynamic model of the unmanned flying platform was thoroughly tested, tested and compared with results obtained, carried out in real conditions during the flight, therefore it is reliable enough to be used as a basis for making selected simulation tests of the model, with the proviso that it does not include all the effects discussed in other author publications, [35], [36].

Modeling of the BSP object has been carried out since the adoption of preliminary assumptions, starting from the determination of the necessary reference systems.

In this respect, two systems were distinguished: the gravitational system (associated with the Earth), which was described by means of four axes $0_e X_e Y_e Z_e$, used to define the movement of a flying object (without taking into account the rotation of the Earth) and the structural system (associated with a flying object), described with axes $0_b X_b Y_b Z_b$, allowing to determine, together with the gravitational system, the spatial position of the flying object, presented by means of the following figure (Fig. 2).

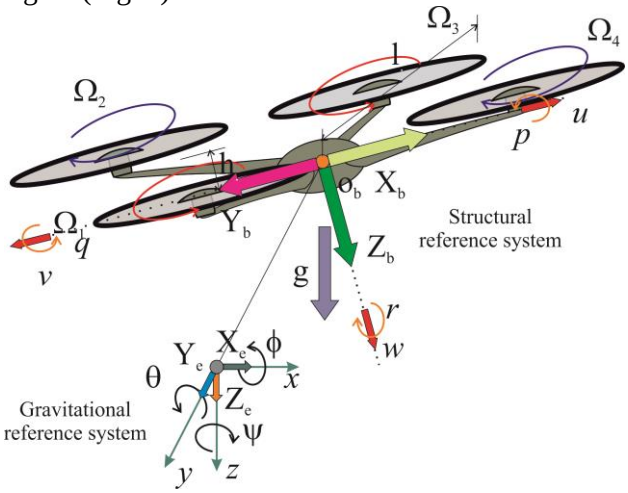

Fig. 2. Reference systems of unmanned flying platform

The current location of the 4-rotor UAV object is defined by three axes *(x, y, z)* with the center of gravity, taking into account the gravity system. However, the current altitude was determined based on the three following Euler angles *(ψ, θ, ϕ)* associated with [37], [38].

- deviation $(-\pi \leq \psi < \pi)$;
- inclination $\left(-\frac{\pi}{2} < \theta < \frac{\pi}{2}\right)$;
- tilting $(-\frac{\pi}{2} < \phi < \frac{\pi}{2})$.

In the further stage of the modeling process, kinematical relations concerning motion and rotation in the inertial reference system associated with the Earth, in relation to the structural system, connected with the unmanned flying platform in the form of a 4-rotor UAV object are presented.

Derivatives with respect to time for *Euler* angles in terms of deviation, inclination and tilting *(ψ, θ, ϕ)* can be expressed in the following form (10):

$$[\dot{\psi}\ \dot{\theta}\ \dot{\phi}]^T = N(\psi, \theta, \phi)\omega, \tag{10}$$

in which $\omega = [p\ q\ r]^T$- define the angular velocities related to the construction reference system, and $N(\psi, \theta, \phi)$ means a matrix that can be expressed in the following form (11):

$$N(\psi, \theta, \phi) = \begin{bmatrix} 0 & sin\phi sec\theta & cos\phi sec\theta \\ 0 & cos\phi & -sin\phi \\ 1 & sin\phi tan\theta & cos\phi tan\theta \end{bmatrix} \tag{11}$$

It should be noted that the matrix (11) depends only on Euler's angles *(ψ, θ, ϕ)* and is reversible in case if its boundaries on *(ψ, θ, ϕ)* are maintained.

Analogously, a derivative with respect to the position time *(x, y, z)* you can specify as (12):

$$[\dot{\psi}\ \dot{\theta}\ \dot{\phi}]^T = N(\psi, \theta, \phi)\omega, \tag{12}$$

where: $V_0 = [u_0\ v_0\ w_0]^T$- defines the current velocity of the 4-rotor UAV object in relation to the Earth system.

In turn, by means of $V = [u\ v\ w]^T$- the current speed of the UAV object, expressed in the reference system related to the flying object, then V and V_0 are related to one another in the following way (13).

$$V_0 = R(\psi, \theta, \phi)\mathrm{V} \tag{13}$$

where: $R(\psi, \theta, \phi)$- they describe the rotation matrix of the unmanned flying platform (14):

$$\mathrm{R}(\psi, \theta, \phi) = \begin{bmatrix} cos\theta cos\psi & (sin\phi sin\theta cos\psi - cos\phi sin\psi) & (cos\phi sin\theta cos\psi + sin\phi sin\psi) \\ cos\theta sin\psi & (sin\phi sin\theta sin\psi + cos\phi cos\psi) & (cos\phi sin\theta sin\psi - sin\phi cos\psi) \\ -sin\theta & sin\phi cos\theta & cos\phi cos\theta \end{bmatrix} \tag{14}$$

For the requirements of building a model of a UAV object, fully compliant with the real flying object, the following simplifications were adopted in the further part of the article: the UAV structure is rigid and symmetrical, the rotors are rigid, and the product of the inertia matrix and the Earth effect can be omitted, [39], [40].

3.1 Forces and aerodynamic moments affecting the engine rotor

By using the blade element theory, you can calculate forces, operating in parallel and perpendicular to the rotor shaft, and aerodynamic moments that affect the shaft and hub of the rotor.

Assuming that the rotors are rigid, the forces acting parallel to the rotor shaft are defined as the rotor thrust T, while forces acting perpendicular to the rotor shaft affect the rotor hub H.

Referring to related issues with moments, on the rotor there were two moments: the moment of resistance M_Q and the torque M_R, but it can be assumed that the force of the rotor operating on the rotor is about a size greater than its resistance.

Respectively, both forces and aerodynamic moments were defined for each rotor. The next figure (Fig. 3) illustrates the forces and aerodynamic moments acting on the engine rotor [10].

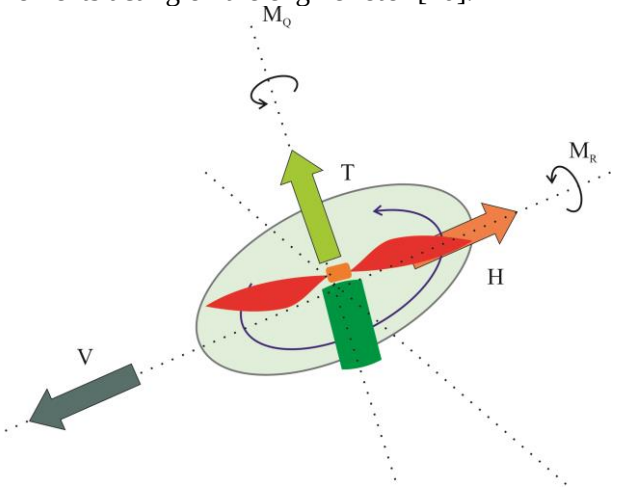

Fig. 3. Forces and aerodynamic moments affecting the engine rotor

The thrust force results from the forces acting on all the elements of the blade in the plane located perpendicular to the rotor shaft, which can be recorded as follows (15):

$$T = C_{T\rho} A(\Omega R)^2$$
$$\frac{C_T}{\sigma a} = \left(\frac{1}{6} + \frac{\mu^2}{4}\right)\theta_0 - (1+\mu^2)\frac{\theta_{tw}}{8} - \frac{\lambda}{4} \tag{15}$$

However, centrifugal force results from the forces acting on all blade elements in the horizontal

plane, the force being zero when the velocity is zero (16).

$$H = C_H \rho A(\Omega R)^2$$
$$\frac{C_H}{\sigma a} = \frac{\mu \bar{C}_d}{4a} + \frac{1}{4}\lambda\mu\left(\theta_0 - \frac{1}{2}\theta_{tw}\right) \quad (16)$$

The moment of resistance results from all the forces acting on the center of the rotor in the horizontal plane, it determines the forces needed to maintain the rotation of the rotor (17).

$$M_Q = C_{M_Q} \rho A(\Omega R)^2$$
$$\frac{C_{M_Q}}{\sigma a} = \frac{1}{8a}(1+\mu^2)\bar{C}_d + \lambda\left(\frac{\theta_0}{6} - \frac{\theta_{tw}}{8} - \frac{\lambda}{4}\right) \quad (17)$$

When considering the tilting moment, it should be noted that due to the fact that the blades move in the horizontal plane in the air, the advancing blade will generate a greater lift force than the returning one, which affects the total torque generated by the rotor, which can be recorded as (18):

$$M_R = C_{M_R} \rho A(\Omega R)^2 R$$
$$\frac{C_{M_R}}{\sigma a} = \mu\left(\frac{\theta_0}{6} - \frac{\theta_{tw}}{8} - \frac{\lambda}{8}\right) \quad (18)$$

3.2 Dynamic equations

Considering the dynamic equations in the area of the 4-rotor UAV object, it was assumed that the vector product of the tensor of the moment of inertia may be omitted in relation to its structure J może być pominięty w odniesieniu do jego konstrukcji (19).

$$J = \begin{bmatrix} I_{xx} & 0 & 0 \\ 0 & I_{yy} & 0 \\ 0 & 0 & I_{zz} \end{bmatrix} \quad (19)$$

Using the general equations of motion (20), (21), recorded in the following form:

$$F_x = -Wsin\theta + X = m(\dot{u} + qw - rv)$$
$$F_y = Wcos\theta cos\psi + Y = m(\dot{u} + ru - pw)$$
$$F_Z = Wcos\theta cos\psi + Z = m(\dot{w} + pv - qu) \quad (20)$$

and

$$M_X = L = I_{xx}\dot{p} + (I_{ZZ} - I_{yy})qr$$
$$M_Y = M = I_{yy}\dot{q} + (I_{xx} - I_{zz})rp$$
$$M_z = N = I_{zz}\dot{r} + (I_{yy} - I_{xx})pq \quad (21)$$

where: F_x, F_y, F_z- they are external forces acting on the frame and M_x, M_y, M_z- are external moments acting on the frame of the 4-rotor UAV object.

In the further part of the paper, external forces and moments acting on the arm of the 4-rotor UAV object were determined [41], [42].

3.2.1 Aerodynamic external forces acting on the arm of 4-rotor UAV object

Forces acting along the axis u	
Centrifugal force	$-\sum_{i=1}^{4} H_{u_i}$
Friction	$-\frac{1}{2}C_u A_u \rho u\lvert u\rvert$
Forces acting along the axis v	
Centrifugal force	$-\sum_{i=1}^{4} H_{v_i}$
Friction	$-\frac{1}{2}C_v A_v \rho v\lvert v\rvert$
Forces acting along the axis w	
Thrust	$-\sum_{i=1}^{4} T_i$
Friction	$-\frac{1}{2}C_w A_w \rho w\lvert w\rvert$

3.2.2 Aerodynamic moments acting on the arm of 4-rotor UAV object

Moments of tilting	
Gyroscope effect of the propeller	$J_r q \Omega_r$
The tilt angle of the servomechanism	$l(-T_2 + T_4)$
The power of inertia caused by traversing flight	$-h\sum_{i=1}^{4} H_{v_i}$
The torque caused by the forward flight	$(-1)^i \sum_{i=1}^{4} M_{R_{u_i}}$
Inclining moments	
Gyroscope effect of the propeller	$-J_r p \Omega_r$
The tilt angle of the servomechanism	$l(T_1 - T_3)$
The power of inertia caused by traversing flight	$h\sum_{i=1}^{4} H_{u_i}$
The inclining moment caused by the forward flight	$(-1)^i \sum_{i=1}^{4} M_{R_{v_i}}$
Moments of deviation	
Inertial moment of inertia	$J_r \Delta\dot{\Omega}_r$
The moment of inertia during Leading out of balance	$(-1)^i \sum_{i=1}^{4} M_{Q_i}$
The forces acting on the hub in the forward flight during leading out of balance	$l\left(H_{u_2} - H_{u_4}\right)$
The forces acting on the hub in thetraverse flight during leading out of balance	$l\left(H_{v_1} - H_{v_3}\right)$

3.2.3 Complete dynamic equations of 4-rotor UAV object

Combining the above equations we get (22):

$$
\begin{aligned}
m\dot{u} &= -m(gsin\theta - qw + rv) \\
&\quad - \sum_{i=1}^{4} H_{u_i} - \frac{1}{2} C_u A_u \rho u|u| \\
m\dot{v} &= m(gcos\theta sin\phi - ru + pw) \\
&\quad - \sum_{i=1}^{4} H_{v_i} - \frac{1}{2} C_v A_v \rho v|v| \\
m\dot{w} &= m(gcos\theta sin\phi - pw + qu) \\
&\quad - \sum_{i=1}^{4} T_i - \frac{1}{2} C_w A_w \rho w|w| \\
I_{xx}\dot{p} &= \left(I_{yy} - I_{zz}\right)qr + J_r q\Omega_r \\
&\quad + l(-T_2 + T_4) \\
&\quad - h\sum_{i=1}^{4} H_{v_i} \\
&\quad + (-1)^i \sum_{i=1}^{4} M_{R_{u_i}} \\
I_{yy}\dot{q} &= (I_{zz} - I_{xx})rp + J_r p\Omega_r + l(T_1 - T_3) \\
&\quad + h\sum_{i=1}^{4} H_{u_i} \\
&\quad + (-1)^i \sum_{i=1}^{4} M_{r_{v_i}} \\
I_{zz}\dot{r} &= \left(I_{xx} - I_{yy}\right)pq + J_r\dot{\Omega}_r \\
&\quad + (-1)^i \sum_{i=1}^{4} M_{Q_i} \\
&\quad + l\left(H_{u_2} - H_{u_4}\right) \\
&\quad + l\left(-H_{v_1} + H_{v_3}\right)
\end{aligned}
\tag{22}
$$

The above dynamic equations (22) constitute a complete model of a 4-rotor UAV object with the previously assumed assumptions. However, it should be noted that despite the negligible impact of several factors (e.g. the occurrence of the Earth effect), after performing appropriate tests, they may be considered when designing next models.

3.2 Dynamic equations of engine

Modelling of engine operation can be based on the following equations:

$$
\begin{aligned}
\dot{\Omega}_m &= -\frac{1}{\tau}\Omega_m - \frac{d}{\eta r^3 J_t}\Omega_m^2 + \frac{1}{k_m \tau}u \\
\frac{1}{\tau} &= \frac{k_m^2}{R_m J_t}
\end{aligned}
\tag{23}
$$

where: d- is the resistance coefficient during hovering, τ- is the time of engine operation, k_m- is constant torque, R_m- is the internal resistance of the engine, η- is the efficiency of the engine and u- is the voltage at the motor input.

By assuming the linearity of the rotor speed around the point Ω_0, the engine speed in hover can be represented as (24):

$$
\begin{aligned}
\dot{\Omega}_m = 0 = -\left(\frac{1}{\tau} + \frac{2d\Omega_0}{\eta r^3 J_t}\right)\Omega_m + \left(\frac{1}{k_m \tau}\right)u \\
+ \frac{d\Omega_0^2}{\eta r^3 J_t}
\end{aligned}
\tag{24}
$$

The relationship between the required angular velocity and the motor voltage is described mathematically in the form (25):

$$
\mathrm{u} = \mathrm{k_m}\tau\left(\left(\frac{1}{\tau} + \frac{2\mathrm{d}\Omega_0}{\eta \mathrm{r}^3 \mathrm{J_t}}\right)\Omega_\mathrm{m} - \frac{\mathrm{d}\Omega_0^2}{\eta \mathrm{r}^3 \mathrm{J_t}}\right). \tag{25}
$$

Then, using the previous equations, you can make the following simplifications (26):

$$
\begin{aligned}
u_{thrust} &= \alpha_{thrust}\sqrt{T} + \beta \\
u_{torque} &= \alpha_{torque}\sqrt{M_Q + \beta}
\end{aligned}
\tag{26}
$$

In addition, the experiments carried out can be used to establish the relationship to calculate the voltage required by the torque and the thrust. Combining previously given patterns, you can get a formula that allows you to calculate the voltage at the output of the motors (27):

$$
\begin{aligned}
u &= \begin{bmatrix} u_{silnik_1} \\ u_{silnik_2} \\ u_{silnik_3} \\ u_{silnik_4} \end{bmatrix} \\
&= k_m\tau\left(\left(\frac{1}{\tau} + \frac{2d\Omega_0}{\eta r^3 J_t}\right)\sqrt{\begin{bmatrix} \frac{1}{4b} & 0 & \frac{1}{2b} & -\frac{1}{4b} \\ \frac{1}{4b} & -\frac{1}{2b} & 0 & \frac{1}{4b} \\ \frac{1}{4b} & 0 & -\frac{1}{2b} & -\frac{1}{4b} \\ \frac{1}{4b} & \frac{1}{2b} & 0 & \frac{1}{4b} \end{bmatrix}\begin{bmatrix} U_1 \\ U_2 \\ U_3 \\ U_4 \end{bmatrix}} - \frac{d\Omega_0^2}{\eta r^3 J_t}\right)
\end{aligned}
\tag{27}
$$

The above equation (27) is implemented to the block responsible for the operation of the motors during the simulation process performed in the Matlab/Simulink program.

8 Results of Simulation Research

The results of calculations of aerodynamic flows of unmanned aircraft are presented below with a drive unit. The calculations were made using the numerical method (FEM), based on formulas in the field of flight mechanics and empirical formulas given, among others in the literature [43], [44]. Simulation tests were performed for the stiffness of the frame, made of plastic weighing 580 grams, having a maximum displacement of 3.4 mm for a pressure of 6.6 N per part of the frame of the wing.

According to the rotor specification given in this test, the distance between the rotor and the analyzed 203x143 mm propeller is 3 mm, while the maximum angular velocity that could be used is 10,000 rpm, generating the thrust of the oscillating thrust after determining a value equal to approx. 6.5 N. This is due to the fact that the air flow between the two the propellers can not penetrate each other, thus creating a stable thrust and not causing vibrations on the body frame.

Simulation tests were carried out for two nozzle cases and without a nozzle. The obtained results of calculations were referenced for different angles of attack of the flowing air. Static configuration was adopted for calculations, i.e. without taking into account the acceleration of the flow in the stream behind the propeller. In turn, in order to examine the effect of the collective air stream on performance, a narrow space was created in the test domain with the drive unit and rotor blades, defining it as so-called tunneling of the drive unit (Fig. 4).

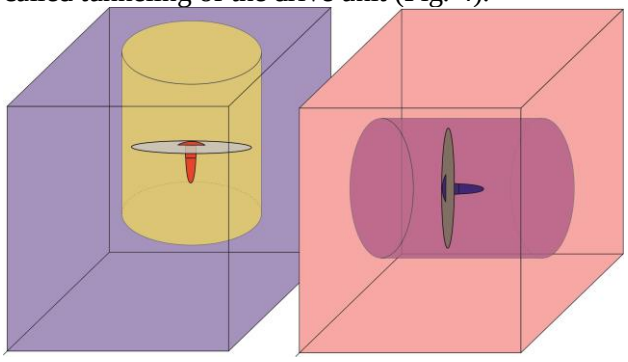

Fig.4. Structure of the UAV object study

With reference to the frame structure of the UAV, the distance between the rotors was selected in the aspect of taking into account the size of the propeller, which is part of the power unit. The size of the propeller and its angular velocity depends on the strength and direction of the air stream produced together with the thrust force. Changes in air flow cause unexpected aerodynamic forces due to changes in atmospheric conditions (strong wind), thrust force and dynamics of propeller blades overlap, [45], [46].

The proposed solution establishes that the opposite pair of propellers will rotate in the same direction as shown in the figure above. This type of solution has limitations as to the maximum size of the propeller that can be used. They result from the maximum rotor torque and the air flow rate generated by each rotor. To achieve flight stability of a quadcopter with respect to airspace, a more efficient solution is to design a support frame, obtaining a control surface that will depend, along with the aerodynamic shape of the rest of the structure of the unmanned aircraft.

The result is the conditions for maintaining flight stability. This can be achieved by minimizing disturbances caused by air swirls in the simulation domain in the research area, as well as by natural phenomena. The quadcopter used in the FEM studies was designed to obtain aerodynamic surfaces in the simulation domain in which drive units were placed, which are used to maintain a steady flight path through the use of air mass masses. The air stream moves relative to the spatial coordinates defined in relation to the UAV object, and then the quadcopter moves with the mass of air flowing through it.

In connection with the above, rotorcraft can react very well to air turbulence. The generated torque inside the quadcopter can be measured based on the technical specification of the rotor used in the UAV object, which is 640 rpm/v, and the maximum voltage used to power the electric motor is approximately 20 V. This means that the maximum rotational speed the rotor is 12180 rpm. In a situation when the quadcopter is equipped with four rotors, with a similar maximum rotational speed and a propeller diameter of 203x143 mm, the maximum wind speed on the propeller is approximately 20 [m/s].

The highest value of wind speed is in the line of the chord that intersects the center of the concurrent drive to the propeller. In addition, air flow is also generated on the outer surface of the propeller rotation, which ranges from 2.6 to 4 [m/s].

It should be noted that it is important to take into account the maximum limitation of the size of the propeller, so that they do not interfere with each other, which would result in a disturbance of the flight dynamics of the quadcopter. In the results of

simulation tests presented below in two cases with or without a nozzle, noticeable changes in the air mass movement can be observed.

In order to better view the aerodynamic phenomena of the air flow in the propulsion unit propeller in the simulation domain within the research area, calculations were made using flow simulation in the *SolidWorks* program for the rotor angular velocity of 10,000 rpm. In the first case, tests were carried out for the variant with strong wind and its lack.

The following drawings (Fig. 5-7) illustrate the pressure distribution on the propeller (Fig. 5), air flow through the propeller (Fig. 6) and the waveform of thrust for the propeller with the nozzle (Fig. 7) for the case without a nozzle together with lack of wind.

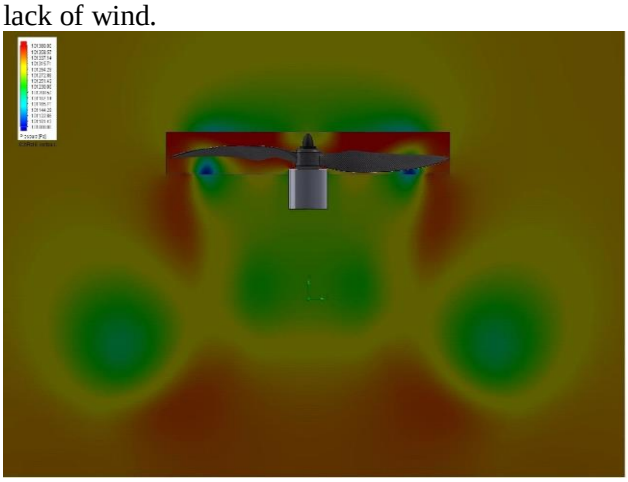

Fig. 5 Distribution of pressure on the propeller without nozzle in the absence of wind

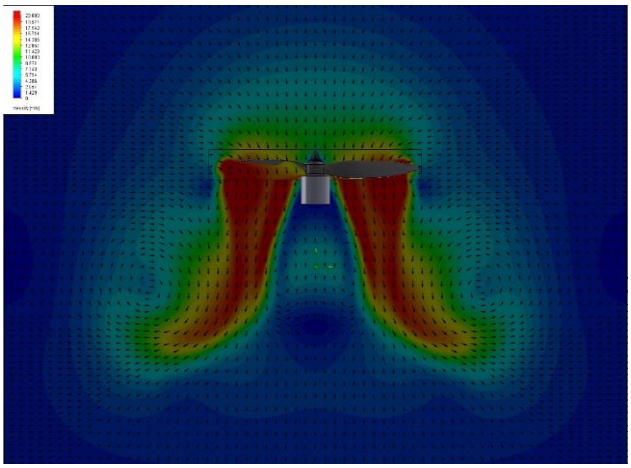

Fig. 6 The flow of air masses through a propeller without a nozzle in the absence of wind

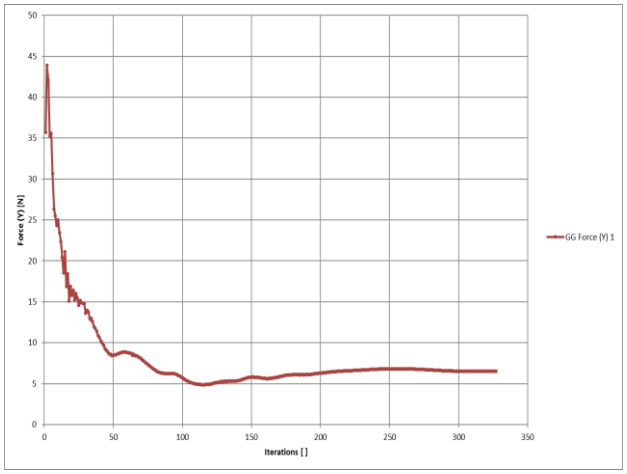

Fig. 7 The waveform of thrust force for a propeller without a nozzle for the case of a lack of wind

At the air inlet of the drive unit with the nozzle around the propeller the absolute velocity of the air and its components are given, in this case the velocity is parallel to the horizontal axis, hence it has no other speed component. The air velocity between the two propellers with the nozzle is marked in yellow. At the maximum angular velocity of the propellers, approximately 50% of the maximum air velocity produced occurs. This large amount of air mass is caused by the oversize propeller or excessive angular velocity.

The numerical results indicate that the presence of the spin speed in the air mass flow field has a significant effect on the efficiency of the quadcopter rotor thrust, while the calculation of the flow dynamics was carried out using the averaged *Reynolds Navier-Stokes* equations. This condition will also cause instability of the thrust generated by each rotor, because the air velocity was influenced by the exhaust air flow in the test domain generated by the surrounding rotor.

Subsequently, the simulations were presented carried out in ideal windless conditions. The propeller unit uses a propeller with 203x143 mm and a 4.5" stroke, and its rotational speed is 10,000 rpm. The next drawings (Fig. 8-10) show the pressure distribution on the propellers, respectively (Fig. 8), air mass flow through the propeller (Fig. 9) and the waveform of thrust for the propeller with the nozzle (Fig. 10) for the nozzle case with the lack of wind.

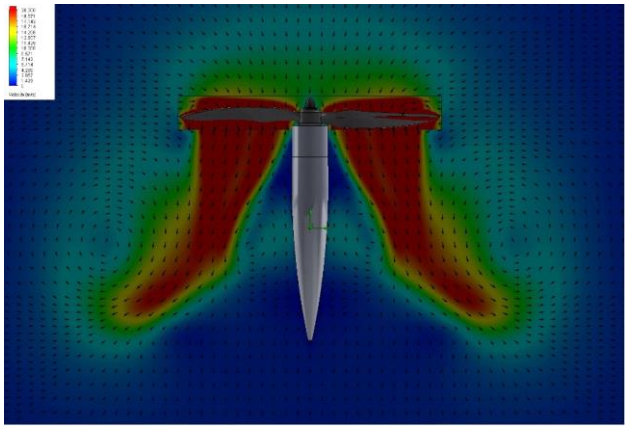

Fig. 8 Pressure distribution on a propeller with a nozzle in the absence of wind

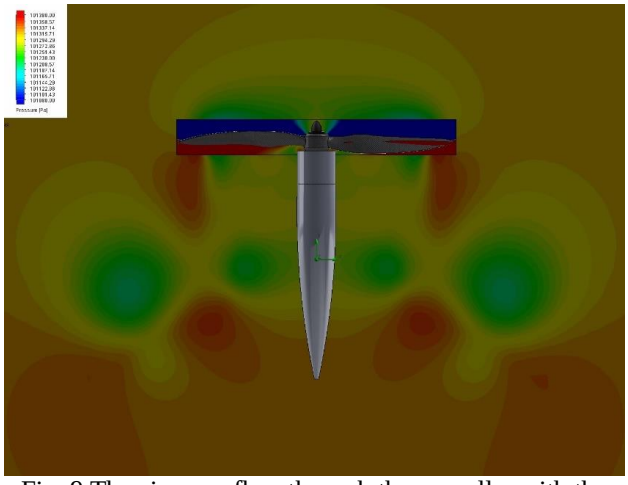

Fig. 9 The air mass flow through the propeller with the nozzle in the absence of wind

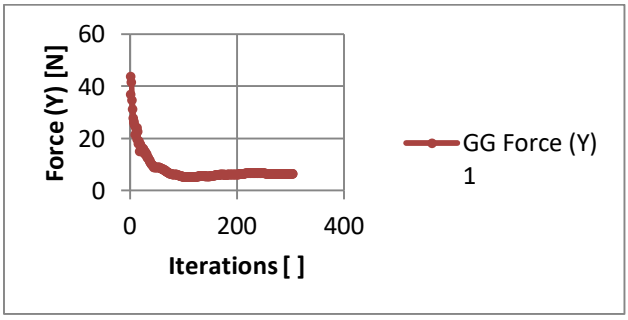

Fig. 10 The waveform of thrust force for a propeller with a nozzle for the case of a lack of wind

Analyzing the above figures, it can be observed that the space between the test domain and the rotor blades was designed in such a way that it was wide enough, i.e. it was possible to change the angle of inclination to 15 degrees, and narrow enough not to affect the characteristics flow. The angle of inclination of the rotor blade is 0 degrees. Speed contours for 0, 4 and 8 degrees of tilt at 10,000 rpm. High velocity air movement in the test domain indicated by the red color suggest an increase in thrust (Figs. 5-6). As the rotational speed of the UAV object propulsion unit increases, the torque increases faster than the thrust [47].

Since the trend line is almost linear, interpolation is possible to find the angle of inclination at other rotational speed values. Lower revolutions for equivalent thrust can lead to lower noise levels. By maximizing the rotational speed of the propeller, the velocity of air flow in the test domain between the two propellers is in the range from 2.1 to 3.6 m/s. In this state, the rotary air in the propeller still affects each other. In the case when the voltage on the rotor is 12 V, the generated rotational motion is 10,000 rpm and the air flow around the propeller can be seen in Fig. 6.

In the figures below (Figures 11-15), for the case of the presence of a side wind with a velocity of 5 m/s, the flow of air masses onto the propeller without a nozzle (Fig. 11) and the nozzle (Fig. 12), pressure distribution on the propeller without a nozzle (Fig. 13) and with the nozzle (Fig. 14) and the waveform of thrust for the propeller with the nozzle (Fig. 15).

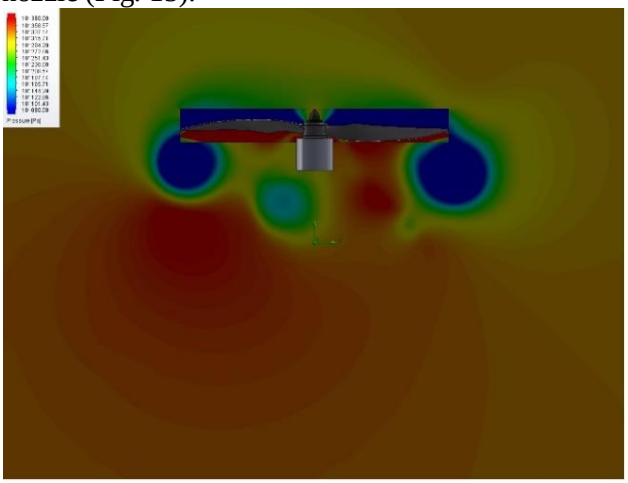

Fig. 11 The flow of air masses on the propeller without a nozzle in the presence of a side wind of 5 m/s

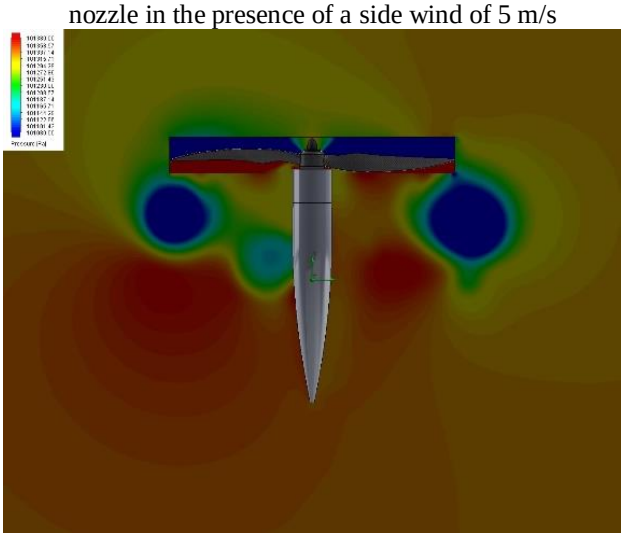

Fig. 12 The flow of air masses on the propeller with the nozzle in the presence of side wind of 5 m/s

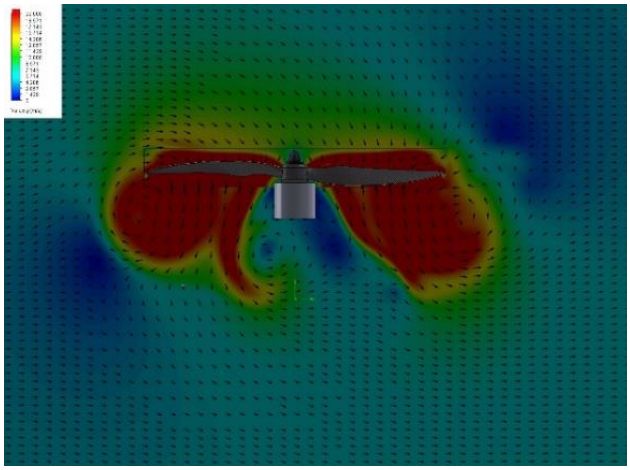

Fig. 13 Distribution of pressure on the propeller without a nozzle in the case of the presence of a side wind with a speed of 5 m/s

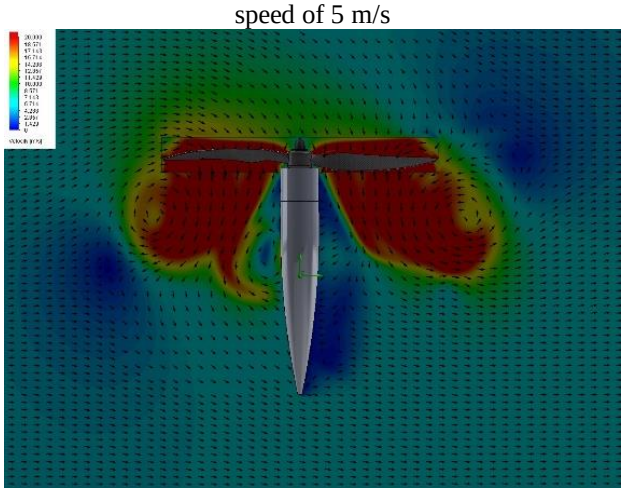

Fig. 14 Pressure distribution on a propeller with a nozzle in the case of the presence of a side wind with a speed of 5 m/s

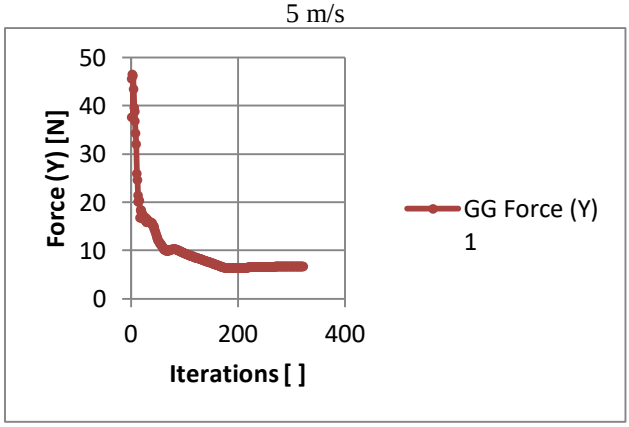

Fig. 15 The waveform of thrust for a propeller with a nozzle for the case of the presence of a side wind with a speed of 5 m/s

To reduce disturbances in the air masses caused by a quadcopter propeller, you can choose a smaller size of the propeller or reduce the regulating voltage on the rotor of the unmanned vehicle, which will translate into a reduction in thrust. The input voltage of 12 V and 7690 rpm will generate air pressure of 6.8 N with a wind speed around the 5 m/s propeller. Other important parameters affecting the air movement are the variable stroke and thrust of the propeller, which can also be analyzed using the calculation method.

9 Conclusions

The presented flow simulations are based on numerical methods. The main problem of this type of simulation is the test mesh *(Mesh)* and appropriate detection of the edge refractions of the object. Therefore, too loose mesh and small density in the vicinity of the body contact causes inaccurate results, while the dense mesh significantly extends the simulation process.

The tests performed in the work were carried out, tested and checked for sagging maneuver, height increase and height reduction under ideal conditions- windless and conditions with side wind at 5 m/s (Figures 11-15). The model is symmetrical with respect to the vertical axis of the entire tested object, therefore the wind occurs only in one of the axes. Checking the operation of the nozzles should be confirmed at different angles of the inclination of the aircraft, which accompany the horizontal flight at the angle of inclination of the unmanned flying platform.

Simulations were carried out using a mesh *(Mesh)* oscillating approx. 3 million points in the area that was obtained by densification of the main domain *(Domain)* by a local domain *(Local Domain)* in the shape of a cylinder, inside which the object was located. The simulation achieved its goal *(Goal)* with the number of iterations *(Iterations)* fluctuating around 100. After achieving the stability of the result, the program stopped the test, which resulted in the end of the simulation at the wrong moment.

A more accurate check of the flow, which requires a much longer time to perform a simulation test, involves the use of time-dependent testing *(Time Dependent)*, thanks to such a solution the authors would avoid simulation errors (Fig. 5-6). The rotational region *(Rotation Region)* also influenced the accuracy of the test results. In the presented simulations, the air masses located in the area rotated relative to the stationary propeller.

In the case of the above simulations, there is no significant impact on the test result, however, in the flow study of the entire UAV object, the propeller should be rotated relative to the fluid in which the simulation is performed. The purpose of using nozzles mounted under the UAV objects engines in a multi-rotor structure is to eliminate the low-pressure centers created under the engine. These

centers cause a negative effect of sucking in newly inflated masses of air and directing them in opposition to the return of the main flow, as a result of which the collision of these masses causes a decrease in the thrust force generated by the drive unit. This kind of construction solution is easy to implement in UAV objects with a multi-rotor structure. It should be noted that the use of nozzles not only affects the aerodynamics of the multi-rotor, but replaces the chassis, which does not increase the weight of the entire structure.

The quadrangular quadcopter body frame structure, which was designed in the *SolidWorks* software, has good stiffness and appropriate dimensions consistent with the specification of the rotor propeller used in simulation tests. For the purpose of preliminary analysis, the generated sequence can be calculated using the theory of momentum and fluid dynamics. However, to get a better result, the experimental method is preferred.

For the purpose of creating mathematical models of the proposed solution, the concept of tunneling in the conducted simulation studies is understood in the context of the simulation domain in the field of research.

References:

[1] M. A. Mahen, S. Anirudh, H. D. Chethana, and A. C. Shashank, *Design and Development of Amphibious Quadcopter*, International Journal of Mechanical and Production Engineering, vol. 2, July 2014, pp. 30-34.

[2] N. V. Hoffer, C. Coopmans, A. M. Jensen, Y. Q. Chen, *A survey and categorization of small low-cost unmanned aerial vehicle system identification*, Journal of Intelligent and Robotic Systems, Vol. 74, No. 1-2, 2014, pp. 129-145.

[3] J. Seddon, *Basic Helicopter Aerodynamics*, BSP Professional Books, London: Oxford, 1990.

[4] R. Austin, *Unmanned Aircraft System*, United Kingdom: Wiley, 2010.

[5] S. H. Jeong and S. Jung, *A quad-rotor system for driving and flying missions by tilting mechanism of rotors: From design to control*, Mechatronics, Vol. 24, No. 8, 2014, pp. 1178-1188.

[6] L. Setlak, R. Kowalik, and W. Redo, *Technological solutions of selected components of energo-electronic power supply system PES in the field of AC/DC/DC in accordance with a trend of more electric aircraft*, In Processing of International Journal of Circuits, Systems and Signal Processing, Vol. 11, 2017.

[7] G. M. Hoffmann, H. Huang, S. L. Wasl and E. C. J. Tomlin, *Quadrotor helicopter flight dynamics and control: Theory and experiment*, In Proceeding. of the AIAA Guidance, Navigation, and Control Conference, 2007.

[8] W. Y. Derrick, S. Nitin, and A. P. Derek, *Onboard Flow Sensing for Downwash Detection and Avoidance with a Small Quadrotor Helicopter*, Proceedings AIAA-Navigation and Control Conference, 2015, pp. 1-11.

[9] L. Setlak, R. Kowalik, and W. Redo, *Study of multi-pulse rectifiers of the PES system in accordance with the concept of a more electric aircraft*, WSEAS Transactions on Systems and Control, Volume 13, 2018.

[10] Edisson Sávio De Góes Maciel, *A Review of Some Numerical Methods to the Euler Equations in Two-Dimensions*, WSEAS Transactions on Fluid Mechanics, Issue 3, Volume 7, July 2012.

[11] Adi Maimun, Saeed Jamei, Agoes Priyanto, Nor Azwadi, *Aerodynamic Characteristics of Wing of WIG Catamaran vehicle During Ground Effect*, WSEAS Transactions on Fluid Mechanics, Issue 1, Volume 5, January 2010.

[12] V. Javir, P. Ketan, D. Santosh, and P. Nitin, Design, *Analysis and Fabrication of Quadcopter*, Journal of The International Association of Advanced Technology and Science, Vol. 16, March 2015.

[13] L. Setlak, R. Kowalik, Studies of 4-rotor unmanned aerial vehicle UAV in the field of control system, MATEC Web of Conferences, Volume 210, 2018.

[14] A. Gessow, and G. C. Myers, *Aerodynamics of the helicopter*, 4th edition Frederick Ungar Publishing Co., 1985.

[15] M. Bangura, R. Mahony, *Nonlinear dynamic modeling for high performance control of a quadrotor*, Australasian Conference on Robotics and Automation (2012), pp. 1-10.

[16] Tsay Tain-Sou, *Model Based Adaptive Controller for Quadrotor UAV with Different Payload*, WSEAS Transactions on Systems and Control, Vol. 17, 2018.

[17] M. Bangura, H. Lim, H. J. Kim, and R. Mahony, *Aerodynamic power control for multirotor aerial vehicles*, In Proceeding IEEE Int. Conference Robotics Automation (2014).

[18] S. Omari, M.-D. Hua, G. Ducard, and T. Hamel, *Nonlinear control of VTOL UAVS incorporating flapping dynamics*, In Intelligent

Robots and Systems (IROS), 2013 IEEE/RSJ International Conference on (2013), IEEE, pp. 2419-2425.

[19] S. Lupashin, and R. D'Andrea, *Adaptive open-loop aerobatic maneuvers for quadro-copters*, IFAC World Congress (2011).

[20] P. Pounds, R. Mahony, and P. Corke, *Small-scale aeroelastic rotor simulation, design and fabrication*, In Proceedings of the Australasian Conference on Robotics and Automation (2005).

[21] R.W. Prouty, *Helicopter performance, stability, and control*, 2002.

[22] D. Pucci, *Flight dynamics and control in relation to stall*, In American Control Conference (ACC), 2012 (2012), IEEE, pp. 118-124.

[23] L. Setlak, R. Kowalik, *The effectiveness of on-board aircraft power sources in line with the trend of a more electric aircraft*, 2018 19th International Scientific Conference on Electric Power Engineering, EPE 2018.

[24] M. J. Cutler, J. P. How (Supervisor), *Design and Control of an Autonomous Variable-Pitch Quadrotor Helicopter*, MIT, Boston, USA, 2012.

[25] H.M. Huang, G.M. Hoffmann, S.L. Waslander, and C. J. Tomlin, *Aerodynamics and control of autonomous quadrotor helicopters in aggressive maneuvering*, in Proceedings of the IEEE, International Conference on Robotics and Automation, IEEE, Kobe, Japan, 2009, pp. 3277-3282.

[26] M. Huang, B. Xian, C. Diao, K. Yang, and Y. Feng, *Adaptive tracking control of underactuated quadrotor unmanned aerial vehicles via backstepping*, In American Control Conference (ACC), pp. 2076-2081, 2010.

[27] W. Zeng, B. Xian, C. Diao, Q. Yin, H. Li, and Y. Yang. *Nonlinear adaptive regulation control of a quadrotor unmanned aerial vehicle*, In Control Applications (CCA), 2011 IEEE International Conference, 2011, pp. 133-138.

[28] K. Mangler, and H. Squire, *The induced velocity field of a rotor*, Tech. Rep. 2642, Aeronautical Research Council, 1953.

[29] M. Bangura, and R. Mahony, *Real-time model predictive control for quadrotors*, In 19th IFAC World Congress, Cape Town, South Africa (2014).

[30] L. Setlak, R. Kowalik, *Study of the transformer rectifier unit compatible with the concept of a more electric aircraft*, 2018 Progress in Applied Electrical Engineering, PAEE 2018.

[31] D. Mellinger, Q. Lindsey, M. Shomin, and V. Kumar, *Design, modeling, estimation and control for aerial grasping and manipulation*, In Intelligent Robots and Systems (IROS), 2011 IEEE/RSJ International Conference, pp. 2668-2673, 2011.

[32] L. Setlak, R. Kowalik, *Analysis, Mathematical Model and Simulation Tests of the Unmanned Aerial Vehicle Control System*, WSEAS Transactions on Systems and Control Vol. 14, pp. 51-56, 2019.

[33] B. Whitehead and S. Bieniawski, *Model Reference Adaptive Control of a Quadrotor UAV*, In Proceeding Guidance Navigation and Control Conference 2010, Toronto, Ontario, Canada, AIAA, 2010.

[34] G. Allibert, D. Abeywardena, M., Bangura, and R. Mahony, *Estimating body-fixed frame velocity and attitude from inertial measurements for a quadrotor vehicle*, IEEE Multi-Conference on Systems and Control (2014).

[35] L. Setlak, R. Kowalik, *Examination of the Unmanned Aerial Vehicle*, ITM Web of Conferences 24, 01006, 2019.

[36] L. Setlak, R. Kowalik, *Evaluation of the VSC-HVDC system performance in accordance with the more electric aircraft concept*, 2018 19th International Scientific Conference on Electric Power Engineering, EPE 2018.

[37] D. Pucci, T. Hamel, P. Morin, and C. Samson, *Nonlinear control of PVTOL vehicles subjected to drag and lift*, In Decision and Control and European Control Conference (CDC-ECC), 2011 50th IEEE Conference on (2011), IEEE, pp. 6177–6183.

[38] P. Pounds, R. Mahony, and P. Corke, *Design of a static thruster for microair vehicle rotorcraft*, Journal of Aerospace Engineering 22, 1 (2009), pp. 85-94.

[39] D. Mellinger, N. Michael, and V. Kumar, *Trajectory generation and control for precise aggressive maneuvers with quadrotors*, The International Journal of Robotics Research 31, 5 (2012), pp. 664-674.

[40] P. Pounds, and S. Driessens, *Towards a more efficient quadrotor configuration*, In Intelligent Robots and Systems (IROS), 2013 IEEE/RSJ International Conference on (2013), IEEE, pp. 1386–1392.

[41] D. Abeywardena, S. Kodagoda, G. Dissanayake, and R. Munasinghe, *Improved state estimation in quadrotor MAVs*, IEEE Robotics Automation Magazine 20, 4, pp. 32-39, 2013.

[42] A. Bramwell, D. Balmford, and G. Done, *Bramwell's helicopter dynamics*, Elsevier Science, 2001.
[43] J. G. Leishman, *Principles of Helicopter Aerodynamics*, Cambridge Aerospace Series, 2002.
[44] L. W. Steven and W. Carlos, *Wind Disturbance Estimation and Rejection for Quadrotor Position Control*, AIAA Conference, , April 2009, pp. 1-14.
[45] B. William, Jr., *A Primer in Fluid Mechanics - Dynamics of Flow in One Space Dimension*, CRC Press, 1999.
[46] K. Van, J. N. Sorensen, and V. L. Okulov, *Rotor Theories by Professor Joukowsky: Momentum Theories*, Aerospace Sciences-Elsevier Journal, 2015, pp. 1-18.
[47] V.-A Luis and N. Jiri, *Computational Analysis of the 2415-3S Airfoil Aerodynamic Performance*, Journal of Systemics, Cybernetics and Informatics, Vol. 12, 2014, pp. 46-51.